XRISE-M: X-radiography facility for solidification and diffusion studies of alloys aboard sounding rockets

F. Kargl,[1, 2, a)] J. Drescher,[1] C. Dreißigacker,[1] M. Balter,[1] M. Becker,[1] M. Wegener,[1] and E. Sondermann[1]
[1)] *Institut für Materialphysik im Weltraum, Deutsches Zentrum für Luft- und Raumfahrt, 51170 Köln, Germany*
[2)] *Foundry Institute, RWTH Aachen University, Intzestraße 5, 52046 Aachen, Germany*

(Dated: 2 December 2019)

A compact fully-protected micro-focus X-radiography facility (XRISE-M) is presented for the study of microstructure evolution during solidification of thin liquid alloy samples and chemical diffusion in liquid binary alloys in-situ and in real-time aboard a sounding rocket. XRISE-M presently enables the simultaneous processing of either two near-isothermal solidification furnaces or a combination of a linear-shear cell diffusion furnace and a near-isothermal solidification furnace. For optimal detector calibration shortly before flight the furnaces can be rotated around the central beam axis and calibration images can be recorded. The facility allows for a pre-heating of the samples into the liquid state prior to lift-off without leakage during the ascent phase at accelerations of up to 27 g. Macro-segregation on re-melting of thin metal samples for microstructure evolution investigations is prevented by an inclinable furnace metric. The use of ion-getter pumps for vacuum generation enables to exploit the entire available time of reduced gravity for image recording and data acquisition. With the device and currently available sample environments microstructure formation upon solidification and chemical diffusion under purely diffusive conditions in alloys can be investigated. The facility can be used equally for other investigations such as granular matter dynamics or metal foaming provided suitable experiment inserts are developed in the future.

I. INTRODUCTION

X-radiography has proven a versatile tool in monitoring metallurgical processes in-situ and in real time. Using X-radiography metal foaming[1,2], alloy solidification[3–14], and chemical diffusion in binary liquid alloys[15–17] have been studied both on ground and in microgravity. In particular, microgravity research requires compact and lightweight facilities that make optimal use of the short periods of processing time available aboard parabolic flights or sounding rockets, or the even more expensive processing time on long-duration platforms such as reentry satellites or the International Space Station (ISS). Recently, X-radiography parabolic flight facilities have been developed at DLR[18] and by Swedish Space Corporation[10,13] both based on the ISS technology demonstrator DIXI[19]. The two facilities show different levels of flexibility. In particular X-RISE has the advantage of enabling a flexible setting of sample orientation with respect to gravity. However, both facilities have in common that they require one or several operators and are quite heavy. For microgravity times of minutes, sounding rockets are the microgravity platforms of choice. Experiments have been recently reported making again use of a sounding rocket X-radiography facility developed by DLR[16] and of a facility developed by Swedish Space Corporation[14,20]. Common to both facilities is that a single experiment could be performed in flight and calibration of the imaging system has to be carried out well ahead of the actual flight in case of SSC's MASER sounding rocket module or as part of a late access activity for the DLR sounding-rocket module used aboard MAPHEUS-4. All facilities obey the respective national laws for safe X-ray operation. All facilities are set-up such that the operators do not have to wear dosimeters due to X-ray emission being well below the applicable maximum allowed dose levels for an effective classification as fully-protected X-ray equipment.

Here, we report on a novel sounding rocket X-radiography facility implemented in a 17" diameter sounding-rocket module environment. The major improvements of this facility compared with earlier reported ones are: 1) Doubling of the science output by enabling to simultaneously process two independent experiment inserts; 2) Increasing the quality of the images by being able to take calibration images only few hours to tens of minutes prior to lift-off without any late access activity required; 3) Enabling a sequence of test solidification experiments on ground prior to lift-off without compromising the sample quality by a frozen in macrosegregation due to the ability to tilt the furnaces. With such test experiments the point of solidification can be precisely targeted to lay within the microgravity time-window even for slow cooling rates and non grain-refined samples. 4) In case of breakage of furnaces or degradation of samples easy replacement via the large hatches implemented in the outer module structure and on the sample environment chamber. This is even possible when the entire payload is in-flight configuration within the launcher.

The paper is structured as follows: First we discuss the technical details of the facility which includes the mechanical design, the electrical design, the sample envi-

[a)] Corresponding author:florian.kargl@dlr.de

ronment chamber, and the detector modules. The technical description of the facility is put to a test by showing results of solidification experiments carried out aboard MAPHEUS-6&7 as well as some results acquired during a diffusion experiment aboard MAPHEUS-5.

II. TECHNICAL DETAILS

Figure 1 shows a photograph of the X-ray sounding-rocket module XRISE-M. The module is in parts made semi-transparent to enable a view on the internal configuration of the sounding rocket module. The XRISE-M module itself has a weight of approximately 95 kg depending on the sample environment used at a total length of 890 mm and an outer diameter of 438 mm.

A. Mechanical Design

The module is centred around a water-cooled mid-deck (cf. Fig. 1 label c) made out of an Al 7075-T6 alloy. The mid-deck separates the part of the module housing the sample environment (top part) from the X-ray and control part (lower part). The part of the sounding rocket module housing the X-ray source and the module control is gas-tight sealed and operates at ambient ground-pressure conditions during flight. This is required to prevent electrical break-through for the high voltage (kV) X-ray source control part. In order to ensure communication between the different parts of the sounding rocket a feed-through cable duct runs through the X-ray part close to the module's side-wall. This feed-through cable-duct is subject to the surrounding pressure environment in flight. When transiting the atmosphere, the outer structure is heated-up to temperatures well above 100 °C. In order to prevent overheating of the components within the sounding rocket module during flight, sheets of flexible cork (3 mm thickness) are covering the internal side-walls of the module. All internal structures are as best as possible isolated from the hot surrounding. This is achieved by fixing all parts to the mid-deck via support struts and intermediate decks made of lightweight composite material. Overall mechanical stability is achieved via the mid-deck plate to which all equipment is fixed. Besides the X-ray source, the control electronics for the X-ray source, a computer (Intel NUC i5 D54250) for driving the entire facility, a NI myRIO-1900 controller for experiment operation, LiFePO4-batteries (I-TECC Headway 3.4V 8Ah) configured in a stack with 27 V and 216 Wh for in-flight operation, an ion-getter pump (VacIon Plus 20 StarCell) sustaining X-ray source vacuum, and valves for vacuum connection to the umbilical on ground as well as to the space environment in-flight are contained. The control part of the module has besides a connector for the vacuum umbilical further vacuum-tight umbilical connectors for communication (RJ-45), for power as well as charging of the batteries, and for cooling water.

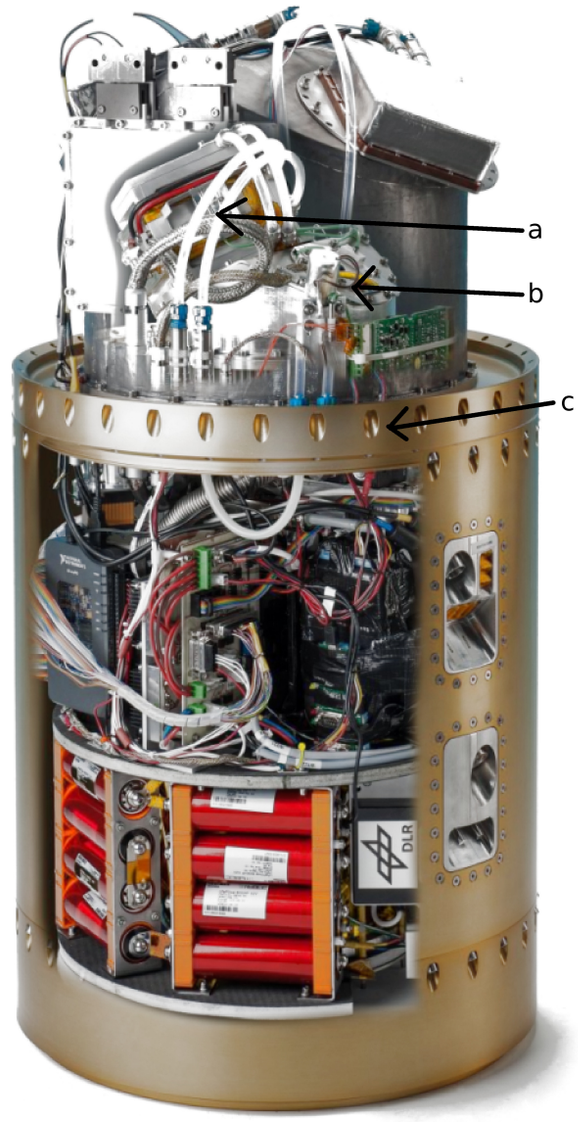

FIG. 1. Photograph of the sounding rocket module XRISE-M. The top outer shell is left away for clarity reasons. The sample-environment chamber at the top as well as the lower outer structure are shown semi-transparent to enable a view onto the sample environment and the X-ray control-part, respectively. In the present configuration: a) a diffusion furnace and b) a near-isothermal solidification furnace are implemented. At the lower right side of the outer structure the umbilical connectors are shown with vacuum and power-connectors at the top and cooling water and RJ-45 connectors at the bottom. c) Mid-deck to which all components are mechanically attached.

B. Electrical Design

Two modes of operation can be generally distinguished: During ground operation, the communication is carried out via Ethernet hardline providing full access to all features of the facility. Hereby, the power to the facil-

ity is supplied via an external power supply via the power umbilical. During flight-operation, communication to the module is sustained via the service module from which all information of the experiments and basic information on module operation are obtained. Full telecommanding of the experiment units and limited commanding of the X-ray facility but not of its control software are possible. In flight power is supplied via a stack of batteries.

For general operation of the facility the compact computer unit is used on which the X-ray control and acquisition software Labex developed by Fraunhofer EZRT as well as the NI control software LabView are running. The LabView interface has been programmed in-house and set up to the required specifications. LabView is used in combination with the myRIO-1900 controller to control the experiment units inside of the processing chamber (temperature PID control), valve operation, power-on/off operation, ion getter pump operation, and turntable as well as furnace rotation stage operation. During count-down and flight, Labex can be operated in an automated count-down mode. The count-down mode is started at a well defined time in the count-down procedure (typically 5 minutes) before lift-off. The program operates according to the set time-line. Upon reaching microgravity conditions the X-ray source is turned on and automated image acquisition is started. In case of X-ray malfunction (over-current etc.) the software automatically attempts to switch on the X-ray source until end of microgravity is reached according to the pre-calculated time-line.

C. Sample environment chamber

The experiment inserts are housed within a stainless-steel chamber. A CAD-schematic of the sample environment is shown in figure 2. The stainless steel chamber (grey-part) is connected to the mid-deck via its circular adaptor ring and vacuum-tight sealed by means of a rubber o-ring slotting into the mid-deck (red dot). The outer diameter of the sample-environment chamber is 310 mm at a wall-thickness of 1 mm. The top-part of the sample environment chamber has two flat faces at an angle of 29.5 degree running opposite to each other effectively constituting an inclined roof (cf. Fig. 2). The entire sample environment chamber is covered in lead-sheet of 2 mm thickness glued to the stainless-steel chamber with adhesive foil. This provides a gap-less shielding of the environment thereby enabling safe X-ray operation on-ground. The lead-shielding is only interrupted at the positions where the detector modules are mounted to enable free-passage of the X-ray beam to the active sensor area. For mechanical stability steel rings have been welded to the chamber connect via two roof-spanning steel brackets. Each active sensor area in the sample environment chamber is covered by a CFRP-window (thin black line) of 0.5 mm thickness. This window is glued to the chamber to seal the chamber vacuum-tight. The window has a low absorption coefficient for X-rays. The chamber itself has

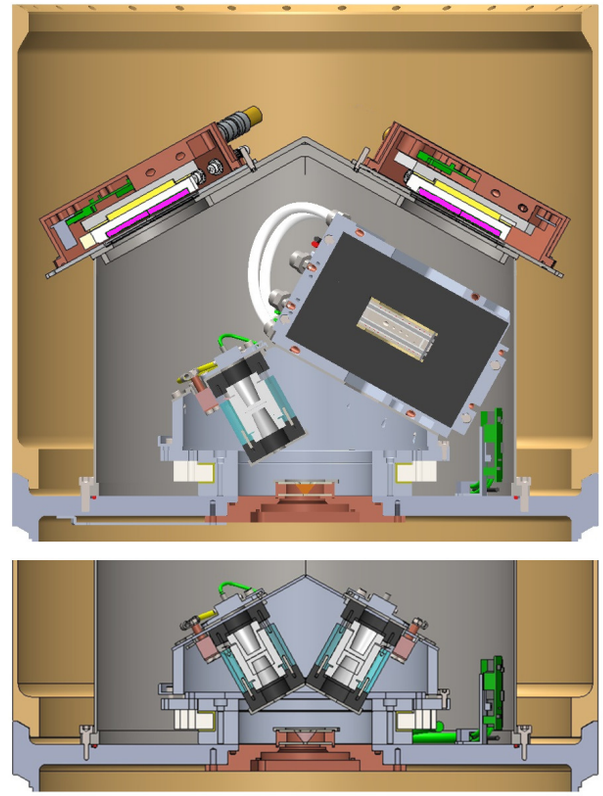

FIG. 2. CAD drawing of upper part of module containing the sample-environment chamber (SEC). Top: SEC with a near-isothermal furnace (left) and shear-cell diffusion furnace (right). Bottom: SCE with two near-isothermal furnaces. The two X-ray detectors (purple) with their Al-baseplate (white) and the Peltier back-cooler (yellow) are placed on top of the inclined roof constituted by the SCE contained in their respective vacuum housings (copper-colored). At the interface to the mid-deck (bottom part) the two X-ray beam defining apertures made out of W-Cu alloy (horizontal grey structures) embedded in copper (copper-colored part) are shown.

no feed-through connectors. All supply lines run with vacuum-tight connectors via the mid-deck directly into the sample environment chamber. Supply lines are available for furnace actuation, furnace power supply, vacuum, cooling-water and thermocouples for temperature control. Outside of the chamber further vacuum-tight feed-through connectors are provided for power and communication to and with the detectors as well as cooling-water connectors for cooling of the detectors.

D. Detector modules

Two scintillator-based X-ray detectors (RadEye2) are used (cf. Fig. 2). The mechanical design is as follows: i) Housing: copper-colored area above the inclined chamber-roof; ii) X-ray detector (purple) in aluminium support (white), which is attached to the copper-housing.

The copper-housings are mounted with a stainless-steel adaptor plate to the sample environment chamber. The detector modules are externally shielded with a 2 mm thick lead-sheet covered by adhesive aluminium foil. The detectors have a 48 μm pixel-pitch with a total active area of 49.3 x 49.2 mm. The detectors can be operated at a maximum frame rate of 2 fps. Typical operation is 0.5 or 1 fps for solidification and for diffusion experiments. The detector-housing is water-cooled. Optionally the X-ray detector module can be further cooled from ambient temperature conditions set by the cooling water-supply using a Peltier cooling element attached to the detector mounting plate (yellow-colored area behind white-colored aluminium support). One of the X-ray detectors uses a standard CsI-scintillator converting X-rays to visible light which is then detected by a CMOS sensor directly-coupled to the scintillator. The second X-ray detector uses a structure scintillator (microstructured Si filled with CsI as a scintillator material described by Svenonius *et al.*[21]) supplied by the company Scint-X. This scintillator strongly suppresses cross-talk between different pixel at the expense of X-ray intensity. The recorded intensity is roughly reduced by a factor of two compared with the detector using the standard scintillator. The X-ray detector modules are connected via an USB-2 interface to the control computer through a connector passing the mid-deck. Power for the detector is supplied via the USB-2 interface. The Peltier-cooler relies on a separate power-connector and has its own control-unit.

III. EXPERIMENTS AND DISCUSSION

The XRISE-M module was successfully tested on ground and passed flight-qualification aboard MAPHEUS-5, MAPHEUS-6, and MAPHEUS-7. On MAPHEUS-5 a near-isothermal furnace for solidification as well as a furnace for measuring chemical diffusion were operated simultaneously. However, X-ray operation ceased about 80 seconds into flight due to overheating of some of the X-ray control electronics and a too-tight restriction on maximum allowed temperatures in software. Even though diffusion coefficients could only be derived in a rather limited way from the data set[17], we show here in subsection III B the general excellent performance of the X-ray facility for diffusion studies. On MAPHEUS-6 & 7 two near-isothermal furnaces containing Al-Ge and Al-Cu samples, respectively, were successfully operated. A sequence of pictures obtained during the flight-experiments and data which can be extracted from these images are shown and discussed.

A. Flight-Operation

Flight-experiments follow a strict timeline. A typical sequence is implementing the samples inside of their furnaces prior to campaign start in the home-laboratory. The furnaces are delivered in gas-tight sealed packaging together with the module itself to the launch site. Several days before launch, the furnaces are implemented into the XRISE-M facility followed by a check-out procedure verifying proper operation of the module. Further tests including a test-countdown are carried out, whereby the samples remain as they were delivered (diffusion experiments) or where additional melting cycles for parameter definition are carried out (solidification). On launch-day the X-ray source is conditioned a few hours before lift-off as part of the nominal check-out procedure. Here, reference images (dark-field, bright-field) are recorded for detector calibration. Typically, the heating-sequence of the furnaces starts 20-30 minutes prior to lift-off with steps of pre-conditioning. Final heating to target temperature is carried out in the last 15 minutes prior to lift-off with fast heating of the furnaces and further checks on sample melting by X-radiography. Automatic mode is activated 5 minutes prior to-lift off for the X-ray source, which follows the set time-line. The X-ray source and image recording are automatically switched-on when microgravity conditions are reached. Image data are only stored onboard and not transmitted to the ground-station due to restrictions in bandwidth. However, experiment control is still possible in flight via telecommanding. Those data are in real-time relayed to and from the ground-station. In case the X-ray source switches itself off in-flight due to e. g. an over-current, a switch-on of the X-ray source is automatically and continually attempted as long as microgravity conditions prevail. Before reentry, the module is completely switched-off to enable safe recovery.

B. Chemical Diffusion Linear Shear-Cell

Al-Cu alloys containing 10 at% to 25 at% Cu in steps of 5 at% were alloyed by weighing in appropriate amounts of raw material and fusing it in a cold-crucible under Argon (99.9999%). Subsequently, a suction casting apparatus (Bühler MAM-1) was used to cast rods of up to 35 mm length and 1.2 mm diameter by first arc melting a spherule of the alloyed material in Argon (99.9999%) atmosphere followed by casting into a water-cooled Cu-mold. The thus obtained rods were subjected to X-radiography to determine the absence of shrinkage holes. Subsequently the rods were cut to appropriate length of about 15 mm. Those rods were implemented in a X-ray transparent linear shear-cell furnace (cf. Ref.[22] for details). The furnace is housed inside of a graphite foam cube. This provides sufficient mechanical stability for linear-shear actuation starting the diffusion process. It also ensures good thermal insulation. In order to not overheat the environment, the graphite-foam cube is mechanically housed within a cube made-out of Al-plates. Water-cooling is implemented as Cu-tubing glued into cut-outs of the Al-plates. On ground, excess heat is transported away from the environment by an active ground-cooling loop. In flight the thermal-mass is suf-

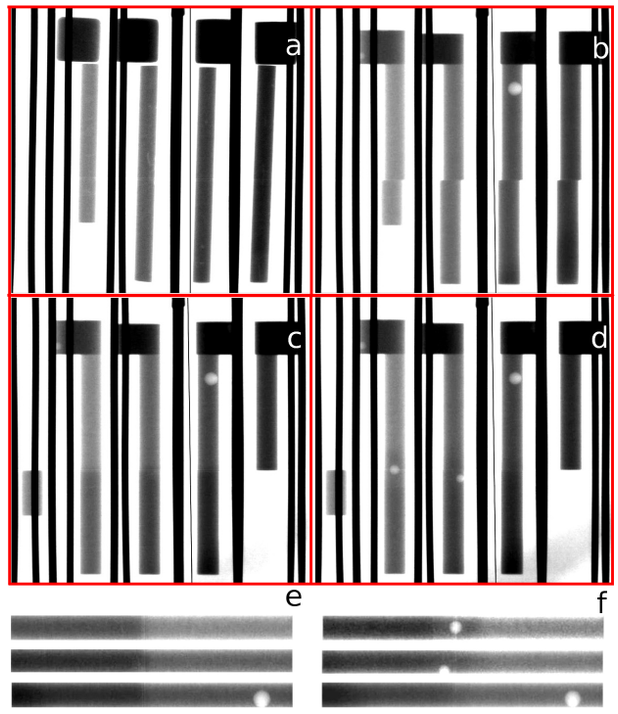

FIG. 3. Sequence of X-radiographs of the linear shear-cell furnace containing four Al-Cu samples with 10 at%, 15 at%, 20 at% and 25 at% Cu (left to right). The composition difference translate into brightness differences with the Cu-richer samples being darker. Samples are shown a) prior to melting on ground; b) after melting on ground; c) 10 s after shear actuation in microgravity; d) 60 s after shear-actuation in microgravity. e) and f) show enlarged and contrast optimized views of the diffusion couples in images c) and d) respectively with left to right translating into top to bottom.

ficient to sustain safe operation without overheating of the environment. For X-ray transmission cut-outs in the Al-plates facing the source and the detector are implemented enabling a free view on the samples. The X-ray source was set to 70 kV acceleration voltage and a beam current of 140 μA. The source-sample distance is 137 mm and the source-detector distance is 240 mm resulting in a magnification factor of 1.75. This leads to an effective per pixel resolution of 27.4 μm.

Fig. 3a-d shows a sequence of recorded radiographs as they were obtained during the MAPHEUS-5 campaign. In Fig. 3a the four Al-Cu alloy samples are visible as they have been integrated into the furnace. The rods are slightly shorter than the capillary cut-outs in the furnace to compensate for volume changes upon heating. On top of each capillary sample 3 mm diameter cylinders are visible. They are made from the same material as the capillary rod and are used as reservoirs to ensure proper capillary filling when the samples are melted. The sample brightness is a measure for the Cu-content, with the brightest sample at the left having the lowest Cu-content of 5 at% and the darkest sample at the right having the

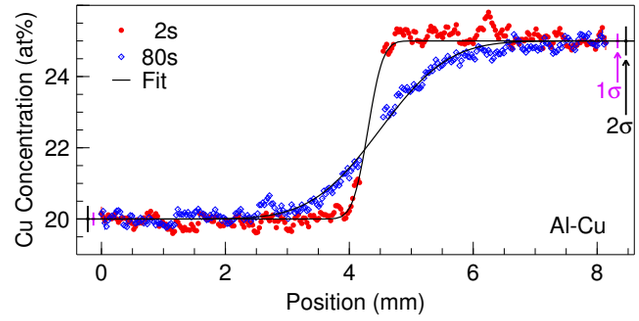

FIG. 4. Concentration profiles determined for the diffusion couple AlCu20at% vs. AlCu25at% 2 s and 80 s after shear-actuation. The solid lines represent a fit to the data using equation 1. The purple and black vertical lines indicate 1σ and 2σ based on the counting statistics and error propagation, respectively.

highest Cu-content of 25 at%. The thick black lines, running vertically through the furnace, correspond to the heating wires. The thin dark line which is 2 pixel wide in the center of the images corresponds to a gap between the two active sensor areas. Figure 3b shows the samples in a fully melted state, whereby the samples are melted on ground and homogenized. It is already visible that the lower part of the furnace can be moved towards the side with respect to the upper part. The minute sliding motion was triggered by shear-rod expansion due to heating. In the Al-Cu20at% sample (third sample from the left) a gas bubble in the upper third of the capillary is visible. Figure 3c shows an image of the furnace taken in microgravity 10 s after shear-actuation. The sample compartments remained without leakage during the ascent phase. It is also visible that diffusion-couples have been obtained whereby bottom and top part containing different Al-Cu alloys are in good contact without leakage at the interface. By the still sharp difference in contrast at the separation line it can be concluded that no major shear-convection occurred. This is due to the slower shear-speed chosen with respect to an earlier measurement on Al-Ni alloys aboard MAPHEUS-4[16]. In Fig. 3d it can be seen from the change in the brightness gradient across the sample compared with Fig. 3c that chemical diffusion 60 s after shear-actuation is well underway. The change in brightness gradient is related to changes in sample composition along the capillary. Furthermore, it can be observed that gas bubbles arose in the left and center capillaries. These bubbles will lead to Marangoni-flow adding to mass transport. Hence, it can be concluded directly from the images at which point in time the diffusion process is likely perturbed. Together with a composition analysis changes in mass transport can be clearly identified.

In order to demonstrate the capability of this facility compared with previous reports from ground experiments[15,23] and a sounding rocket experiment[16] the right capillary which showed a bubble only towards the

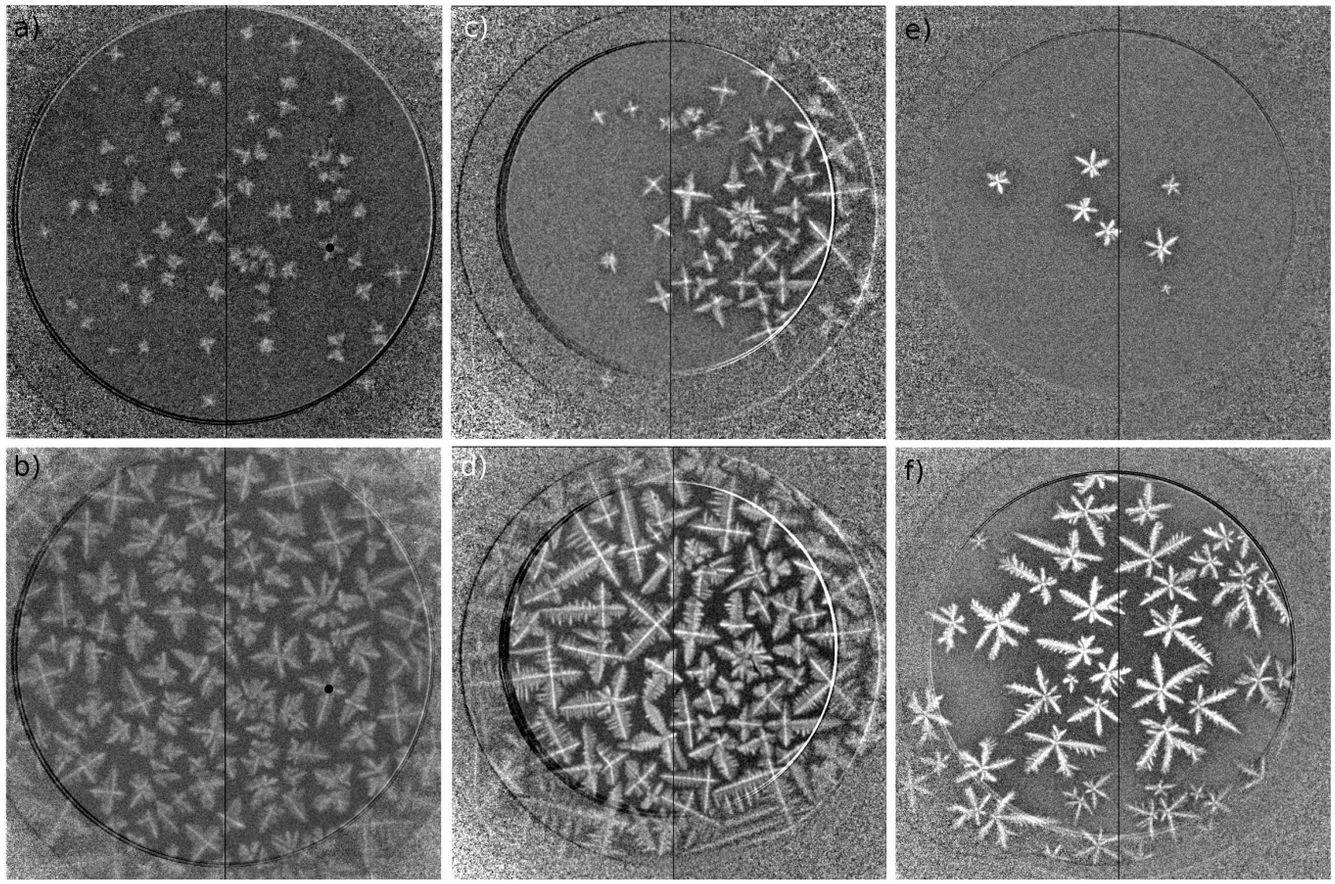

FIG. 5. Image sequence of the solidification of a-d) Al-Cu7at% aboard MAPHEUS-7 and e-f) Al-Ge24at% aboard MAPHEUS-6. For MAPHEUS-7 data of two furnaces are shown: Furnace 2 images a) and b) and furnace 1 images c) and d). The central black line indicates the splitting between the 2 CMOS sensors. For images a) and b) only part of the recorded detector image is shown. For c)-f) a larger area of the recorded image is shown. The first circle marks the inside of the BN-piston the second circle the outside of it. For furnace 1 (c,d) due to the larger detected-intensity Cu-enrichment around the growing dendrites is better visible. For furnace 2 the growing dendrites are sharper but the noise in the image is larger. In a) and b) the later analyzed dendrite is marked with a black dot. For furnace 1 (c,d) the temperature was less homogeneous leading to preferential nucleation on one side of the furnace. With Ge being the heavier element than Cu and the larger amount of Ge, the dendrites and the solutal field are better resolved as shown in images e) and f).

top was analyzed with the result published by Sondermann *et al.*[17]. From the recorded images concentration profiles can be derived following procedures outlined in Ref.[23].The data shown in figure 4 were derived from the AlCu20at%-AlCu25at% diffusion couple. The data were taken approximately 4 mm either side of the shear-interface and well below the bubble visible in the liquid column. The data are shown integrated over the entire width of the liquid column. Data are shown 2 s after shear-actuation where virtually no diffusion has taken place and 80 s after shear where the sharp concentration step has already significantly broadened due to chemical diffusion. In addition to the raw data, Fig. 4 shows also a fit to each data-set represented by a solid line. The fit is based on the following solution of Fick's second law of diffusion assuming an infinitely long diffusion couple:

$$C(x,t) = \frac{C_1 + C_2}{2} - \frac{C_2 - C_1}{2} erf\left\{\frac{x - x_0}{\sqrt{4Dt}}\right\}. \quad (1)$$

Hereby C_i equals to the initial Cu-concentration of the each of the two samples constituting the diffusion couple, erf represents the error function, x_0 defines the zero-flux plane, D is the chemical diffusion coefficient, and t the experiment time. For the fit C_i were kept fixed and $4Dt$ was used as a fit parameter representing the square of the diffusion length. However, the number of data-points available make a proper fit for deriving diffusion coefficients by linearly scaling the fit parameter 4Dt with time difficult. Nevertheless, it is shown that XRISE-M facility enables the measurement of the chemical diffusion process in real-time and that the relevant data can be extracted from the recorded images.

C. Equiaxed-dendrite growth near isothermal furnace

AlCu7at% samples and AlGe24at% samples were prepared from Al (99.9999% Hydro Aluminium), Cu (99.99% Alfa Aesar), and Ge (semi-conductor grade by IKZ Berlin). AlCu7at% was prepared by induction melting in a cold crucible in Argon (99.9999% purity) followed by casting of a rod into a Cu-mold. AlGe24at% was prepared in a conventional small casting furnace in an Argon-filled glove-box inside of a graphite crucible. The melt was stirred for homogenization and cast into a boron-nitride spray-coated stainless steel mold. The cast rods were sectioned and the disc-shaped samples were polished to 200 μm thickness. Subsequently the circular samples of $\sim$12 mm diameter were integrated into a near-isothermal furnace whose working principle and general outline is described by Becker et al.[24]. The furnaces as they have been implemented into the sample environment chamber aboard MAPHEUS-6&7 are shown in Fig. 2. For the experiments the X-ray source was set to 70 kV acceleration voltage and 134 μA beam current. With a source-to-sample distance of 75 mm and a source-to-detector distance of 240 mm a magnification of 3.2 is achieved resulting in an effective pixel size of 15 μm. Images were recorded with 1 fps.

A typical experiment consists of three stages: Preheating, heating to target temperature including annealing, and finally controlled-cooling for the observation of microstructure formation upon solidification. The first two stages are entirely carried out on ground prior to lift-off. The controlled-cooling is also started on ground continuing into the flight. For the here chosen non-grain refined samples it is particularly critical to have a precise idea about the start of nucleation. This is required because the start of cooling from annealing temperature has to be defined such that nucleation and crystal growth take place well within the available microgravity time-window of $\sim$360 s only. To define precisely the starting point of nucleation, several test-runs of solidification on the flight sample are required to be carried out on ground. For these test-runs the controlled-cooling profile as planned in the flight experiment is followed repeatedly intermitted by heating cycles to the annealing temperature after nucleation and growth have been observed. Hereby, the sample is remelted. In X-radiography observation mode the sample plane is inclined by 29.5 deg with respect to the vertical direction, when the payload is integrated in the launcher. In this configuration macrosegregation would lead to an inhomogeneous sample composition as a result of repeatedly melting and freezing of the sample. The reason is that the less dense fcc-Al dendrites would float whereas the denser liquid would segregate in opposite direction. Quick and immediate reheating could alleviate macrosegregation during thermal cycling, however, the final cooling step to ambient ending the test-runs leaves sufficient time for macrosegregation. Hence, the furnace holders are designed such that they can be tilted from their inclined position to a vertical position to avoid macrosegregation on this final cooling step ending the test-runs. An inclination of -5 deg in opposite direction is also possible enabling to homogenize a partly segregated sample. For AlGe24at% 3 K min^{-1} had to be chosen as cooling rate due to the larger uncertainty in initial undercooling. For AlCu7at% a cooling rate of 1 K min^{-1} was selected due to its well defined nucleation undercooling.

A sequence of images of the experiments is shown in Fig. 5. For the Al-Cu7at% samples a larger grain density can be observed Fig. 5a-d). Also the fcc-Al dendrites grow as expected in $\langle 100 \rangle$ direction as indicated by their predominantely four-fold symmetry and 90 deg angle between the primary and the secondary dendrite arms. Some dendrites, in particular in Fig. 5a,b) show a more complex morphology than a regular cross. This can be attributed to the fact that the sample has a finite size in beam direction. In a recent publication by Becker et al.[25] for hypo-eutectic Al-Ge alloys it was shown that depending on the initial grain orientation different growth morphologies for fcc-Al can develop. For Al-Cu for an fcc-Al dendrite in 3D it is expected that six arms along the $\langle 100 \rangle$ directions are growing of which four are visible if the dendrite is perfectly aligned within the thin sample dimension. If the alignment is not perfect and the growing arms lock the growing dendrite in the thin sample direction more than four arms with odd angles can be observed. For the Al-Ge24at% sample shown in Fig. 5e-f) fewer grains are observed even for the faster cooling rate of 3 K min^{-1}. Moreover, fcc-Al grows in $\langle 110 \rangle$ direction as indicated by the six-fold symmetry and a 60 deg angle between primary and secondary dendrite arms. Deviations from six-fold symmetry - ideally valid for a 2D sample and crystals in a $\{111\}$ orientation - can again be rationalized by the finite thickness of the sample and different crystal orientations. This is inline with the earlier in-depth discussion on the crystal growth orientation selection for Al-Ge by Becker *et al.*[25] based on ground experiments. Here, we demonstrate that no difference can be observed in microgravity. From the in-situ X-radiographs also statistics on the nucleation of dendrites can be obtained. However, this is not discussed here.

As shown in Fig. 6 the time-evolution of the dendrite tip can be nicely followed from which dendrite arm length (DAL) and subsequently dendrite-tip velocities (DTV) can be derived. In Fig. 6 top a series of despeckled and noise filtered images are shown, whereby the dendrite outline was determined via the particle-tracking tool of ImageJ. The central graphs in the image show the DAL as a function of time. The data were obtained by manually tracking of the dendrite tip using unfiltered images whereby for noise reduction 5 images of the original 1 fps image sequence have been averaged. The data show that the arms length are steadily increasing. Labels in the graphs correspond to the dendrite arms as labelled in the right image of the time sequence. Arms #2 and #3 stop to grow earlier due to soft impingement with neighbouring arms. The bottom graph demonstrates that dendrite

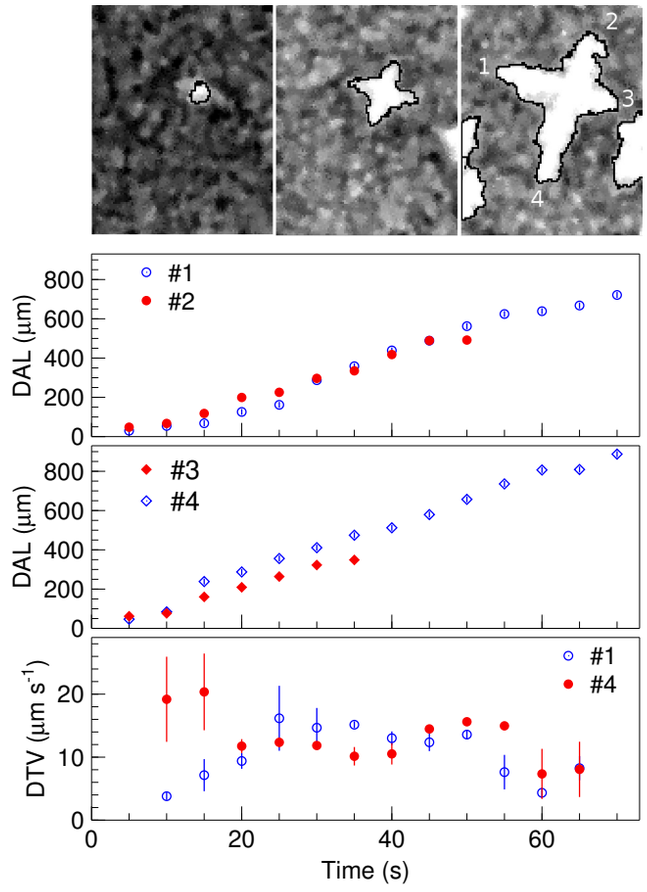

FIG. 6. Top: Image series of a single dendrite taken from the Al-Cu7at% experiment aboard MAPHEUS-7 [cf. black dot in Fig. 5a,b)]. The images have been despeckled and noise filtered for outliers. The black curves indicate the outlines of the dendrites as determined with the particle-tracking tool of ImageJ. Center graphs: Dendrite center-to-tip distance (DAL) as a function of time derived from the image data. Bottom: Dendrite-tip velocities (DTV) as function of time derived by linear fitting 10 s time intervals of DAL.

tip velocities (DLV) can be obtained from the data. To derive tip-velocities a linear fit over 15 s intervals was applied to the DAL data. Error bars are shown as given from the fit to the data. We show only data for the longest dendrite arms #1 and #4. Arm #1 is initially freely growing indicated by the steadily increasing tip velocity. At about 25 s after the dendrite became visible the tip velocity is stagnating and then slowly decreasing due to soft impingement with neighbouring grains. For dendrite arm #4 the initial velocity is quite high though with large error bars due to the noise in the data making a tip determination for arm #4 difficult. Ignoring these first two data points a relatively similar behaviour is observed as for arm #1. The here reported data for tip velocities are in the same range as data earlier reported by Bogno *et al.*[26] for equiaxially growing Al-Cu4.5at% dendrites.

IV. CONCLUSION AND OUTLOOK

A novel compact and fully-protected X-radiography facility XRISE-M for 17"-diameter sounding rockets was presented. XRISE-M records images from the first second of microgravity onward in an automated way. A shear-cell diffusion furnace in combination with a near-isothermal solidification furnace or two near-isothermal solidification furnaces can be currently implemented and simultaneously processed. It was shown that samples can be melted and homogenized on ground before lift-off without any leakage of the liquid during the acceleration phase of the rocket. The capability of the facility was demonstrated by discussing a diffusion and several solidification experiments carried out during the MAPHEUS-5 to MAPHEUS-7 flights whereby images could be taken right at the start of the microgravity phase.

ACKNOWLEDGMENTS

We thank the teams of DLR Mobile Rocket Base (MORABA) and of Swedish Space Corporation (SSC) for their excellent service in making the MAPHEUS campaigns a success. We thank Hydro Aluminium Bonn for providing us with the high-purity Aluminium. We thank the team of the workshop M. Nell, K. Afanasev, H. Esser, and R. Henrichs for their excellent work in converting the mechanical design into operable parts. Th. Gruhl and M. Santourian of FineTec FineFocus Technologies GmbH as well as A. Ennen, S. Reisinger, M. Schmitt, and T. Wörlein of Fraunhofer EZRT are thanked for their remote support before and during the campaign concerning X-ray source and software, respectively.

REFERENCES

[1]F. Garcia-Moreno, M. Fromme, and J. Banhart, Advanced Engineering Materials **6**, 416 (2004).
[2]P. Holm, Y. Houltz, O. Lofgren, P. Andersson, and F. Garcia-Moreno, ESA Special Publications **647**, 385+ (2007).
[3]R. Mathiesen, L. Arnberg, F. Mo, T. Weitkamp, and A. Snigirev, Physical Review Letters **83**, 5062 (1999).
[4]H. Yasuda, I. Ohnaka, K. Kawasaki, A. Suglyama, T. Ohmichi, J. Iwane, and K. Umetani, Journal of Crystal Growth **262**, 645 (2004).
[5]R. H. Mathiesen and L. Arnberg, Acta Materialia **53**, 947 (2005).
[6]R. H. Mathiesen, L. Arnberg, P. Bleuet, and A. Somogyi, Metallurgical and Materials Transactions A - Physical Metallurgy and Materials Science **37A**, 2515 (2006).
[7]S. Boden, S. Eckert, B. Willers, and G. Gerbeth, Metallurgical and Materials Transactions A - Physical Metallurgy and Materials Science **39A**, 613 (2008).
[8]H. Nguyen-Thi, L. Salvo, R. Mathiesen, L. Arnberg, B. Billia, M. Suery, and G. Reinhart, Comptes Rendus Physique **13**, 237 (2012).
[9]A. Murphy, D. Browne, W. Mirihanage, and R. Mathiesen, Acta Materialia **61**, 4559 (2013).

[10]A. G. Murphy, J. Li, O. Janson, A. Verga, and D. J. Browne, Materials Science Forum **790-791**, 52 (2014).
[11]W. U. Mirihanage, K. Falch, I. Snigireva, A. Snigirev, Y. Li, L. Arnberg, and R. Mathiesen, Acta Materialia **81**, 241 (2014).
[12]A. Murphy, W. Mirihanage, D. Browne, and R. Mathiesen, Acta Materialia **95**, 83 (2015).
[13]L. Abou-Khalil, G. Salloum-Abou-Jaoude, G. Reinhart, C. Pickmann, G. Zimmermann, Y. Houltz, J. Li, O. Janson, and H. Nguyen-Thi, ESA Special Publications **730**, 279 (2015).
[14]A. Murphy, R. Mathiesen, Y. Houltz, J. Li, C. Lockowandt, K. Henriksson, N. Melville, and D. Browne, Journal of Crystal Growth **454**, 96 (2016).
[15]B. Zhang, A. Griesche, and A. Meyer, Physical Review Letters **104**, 035902 (2010).
[16]E. Sondermann, F. Kargl, and A. Meyer, Physical Review B **93**, 184201 (2016).
[17]E. Sondermann, N. Jakse, K. Binder, A. Mielke, D. Heuskin, F. Kargl, and A. Meyer, Physical Review B **99**, 024204 (2019).
[18]S. Klein, D. Bräuer, M. Becker, A. Knipstein, S. Meckel, E. Sondermann, and F. Kargl, International Journal of Microgravity Applications **33**, 330405 (2016).
[19]F. Kargl, M. Balter, C. Stenzel, T. Gruhl, N. Daneke, and A. Meyer, Journal of Physics Conference Series **327**, 012011 (2011).
[20]Y. Houltz, J. Li, H. Nguyen-Thi, G. Reinhart, G. Abou Jaoude, R. Mathiesen, D. Browne, A. Murphy, and G. Zimmerman, ESA Special Publications **721**, 275 (2013).
[21]O. Svenonius, A. Sahlholm, P. Wiklund, and J. Linnros, Detectors and Associated Equipment **607**, 138 (2009).
[22]K. Binder, F. Kargl, and C. Stenzel, Review of Scientific Instruments (submitted).
[23]F. Kargl, E. Sondermann, H. Weis, and A. Meyer, High Temperatures: High Pressure **42**, 3 (2013).
[24]M. Becker, C. Dreißigacker, S. Klein, and F. Kargl, Review of Scientific Instruments **86**, 063904 (2015).
[25]M. Becker, J. A. Dantzig, M. Kolbe, S. T. Wiese, and F. Kargl, Acta Materialia **165**, 666 (2019).
[26]A. Bogno, H. Nguyen-Thi, G. Reinhart, B. Billia, and J. Baruchel, Acta Materialia **61**, 1303 (2013).

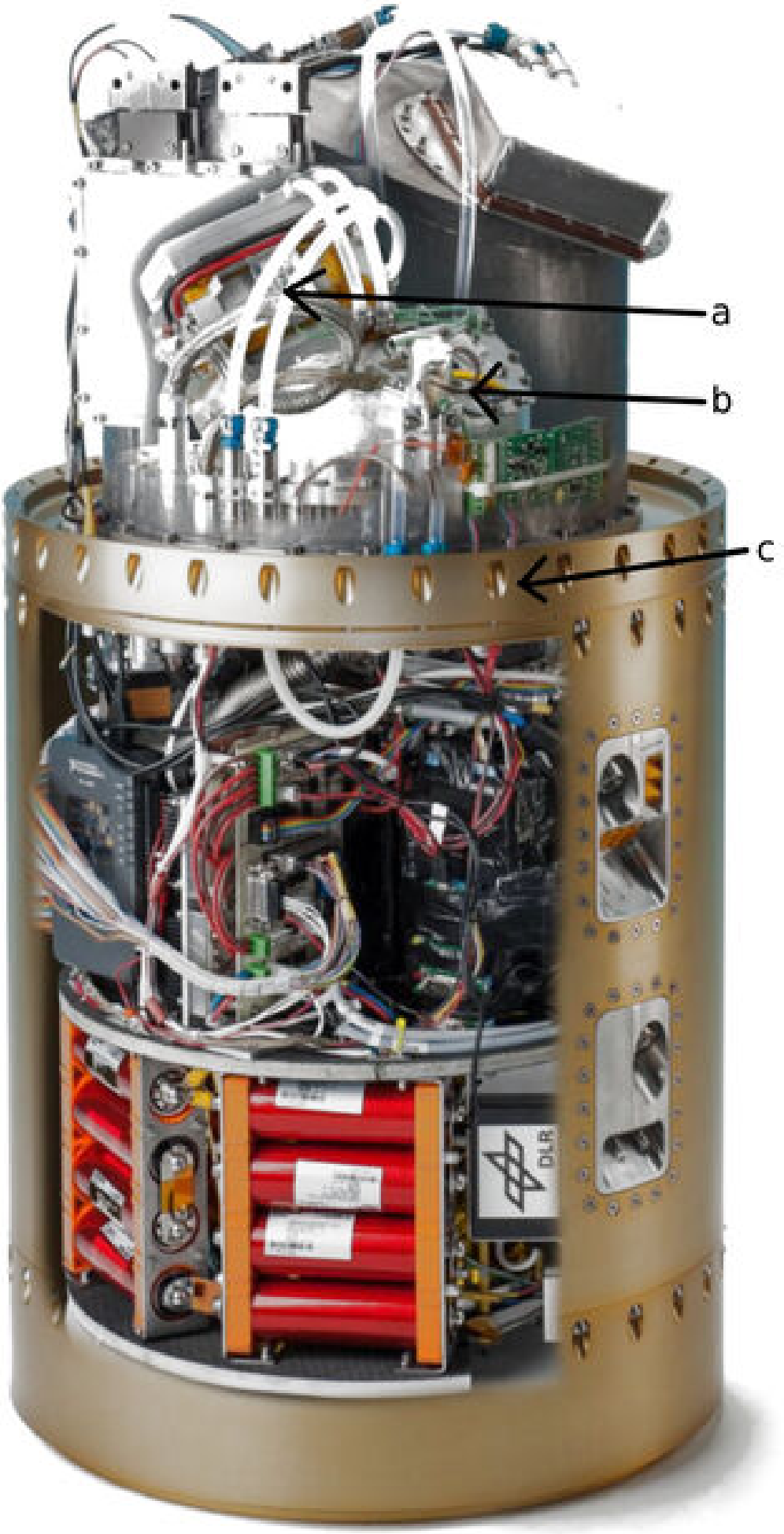
a
b
c
DLR

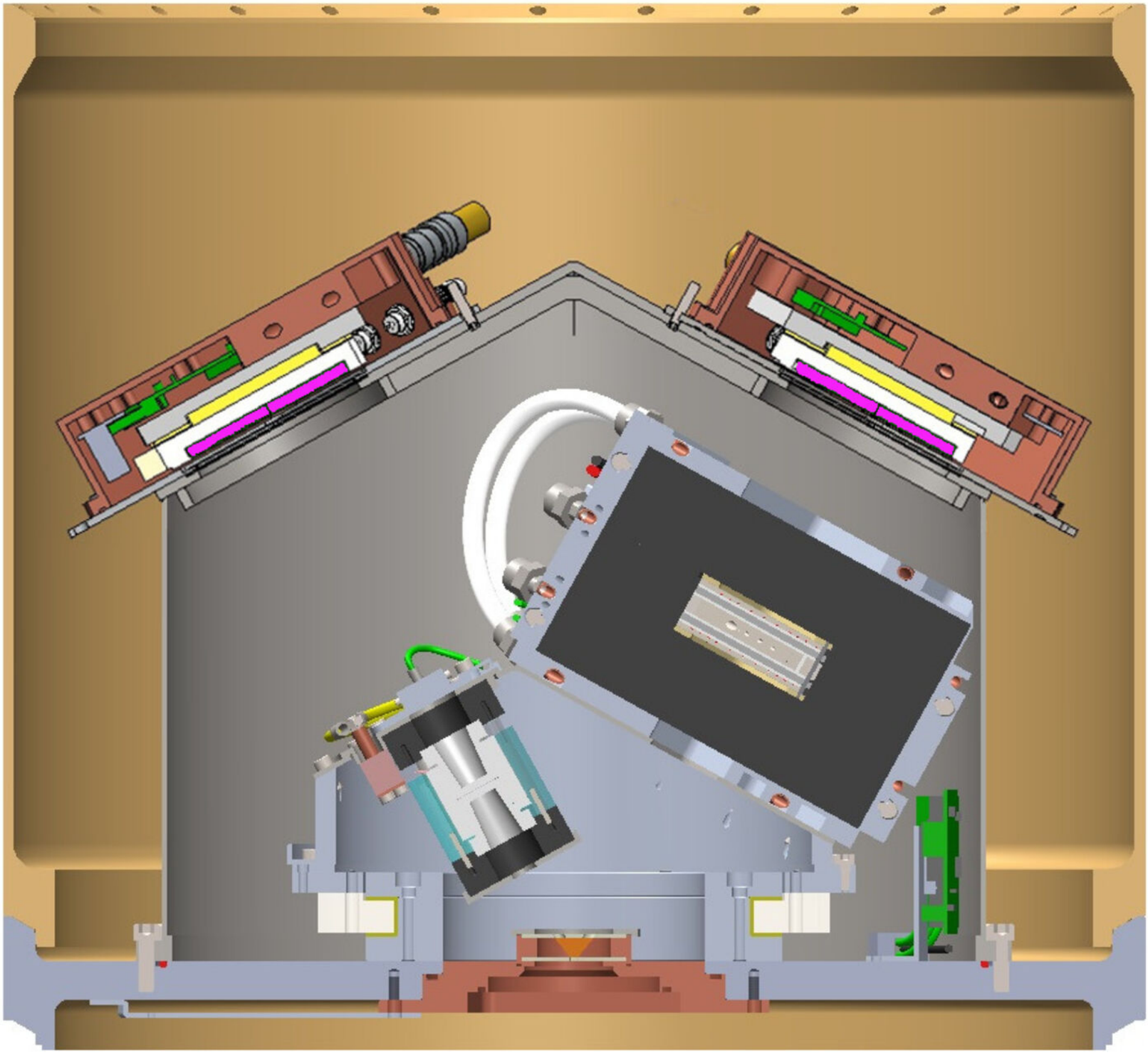

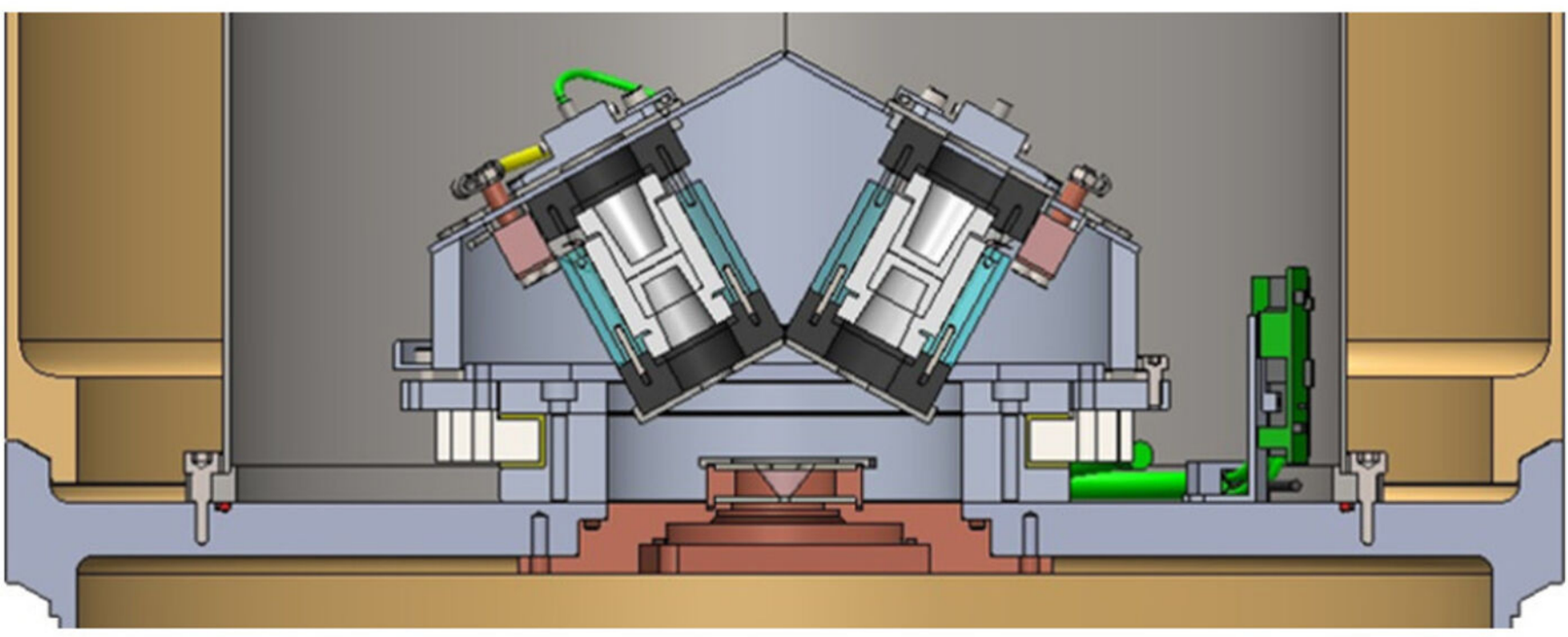

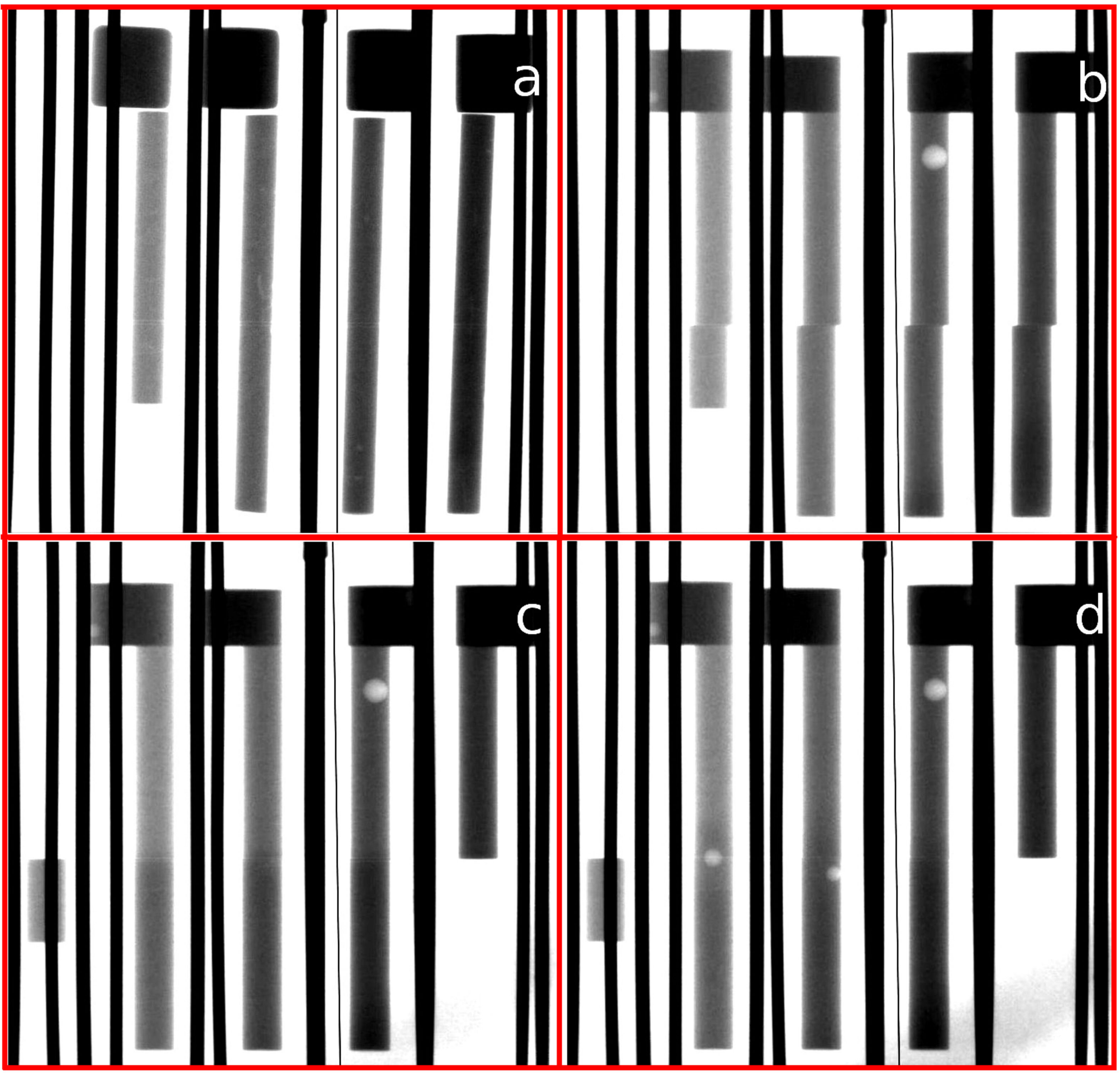
a
b
c
d
e
f

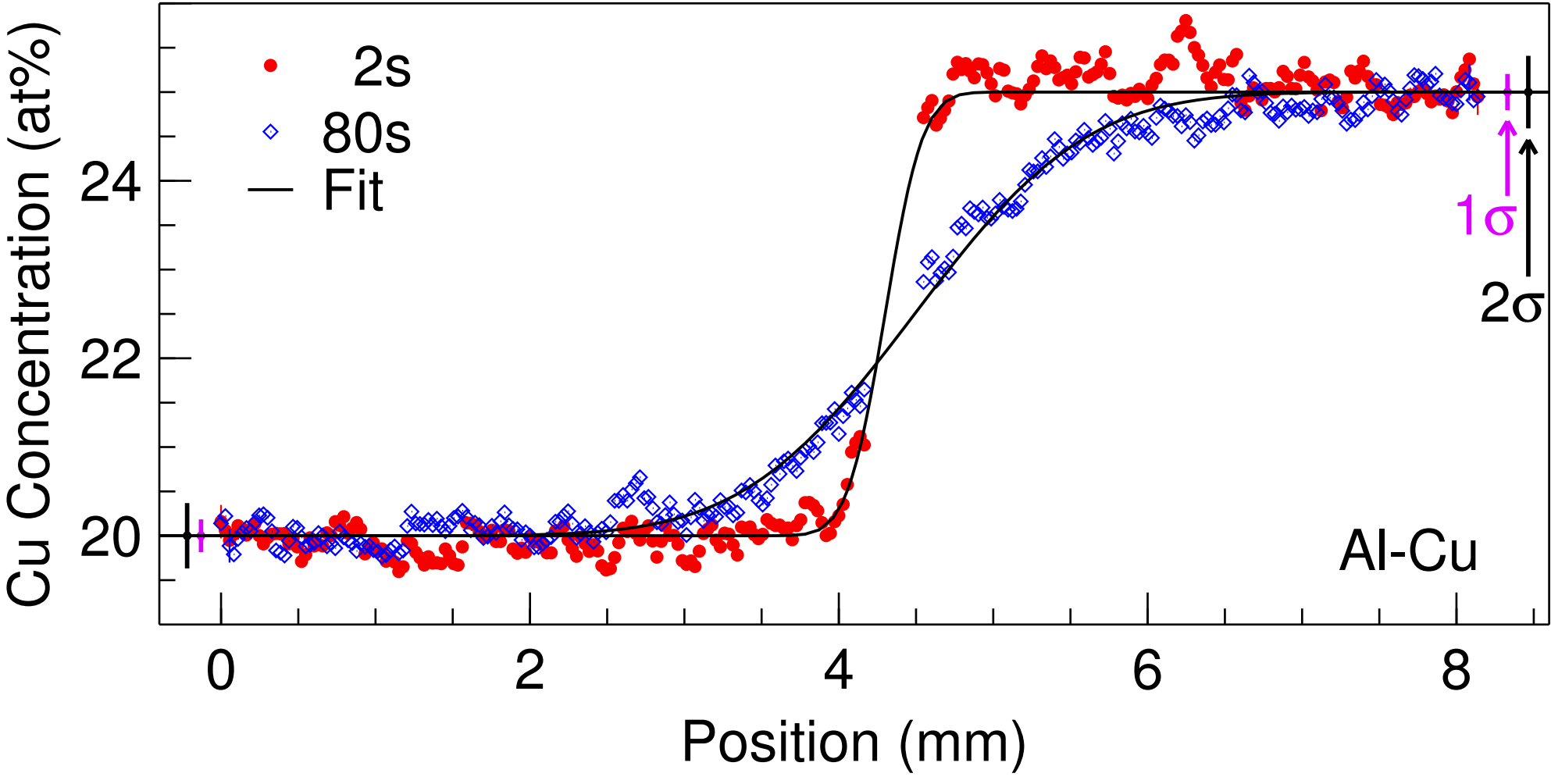
2s
80s
Fit
Cu Concentration (at%)
20
22
24
0
2
4
6
8
Position (mm)
1σ
2σ
Al-Cu

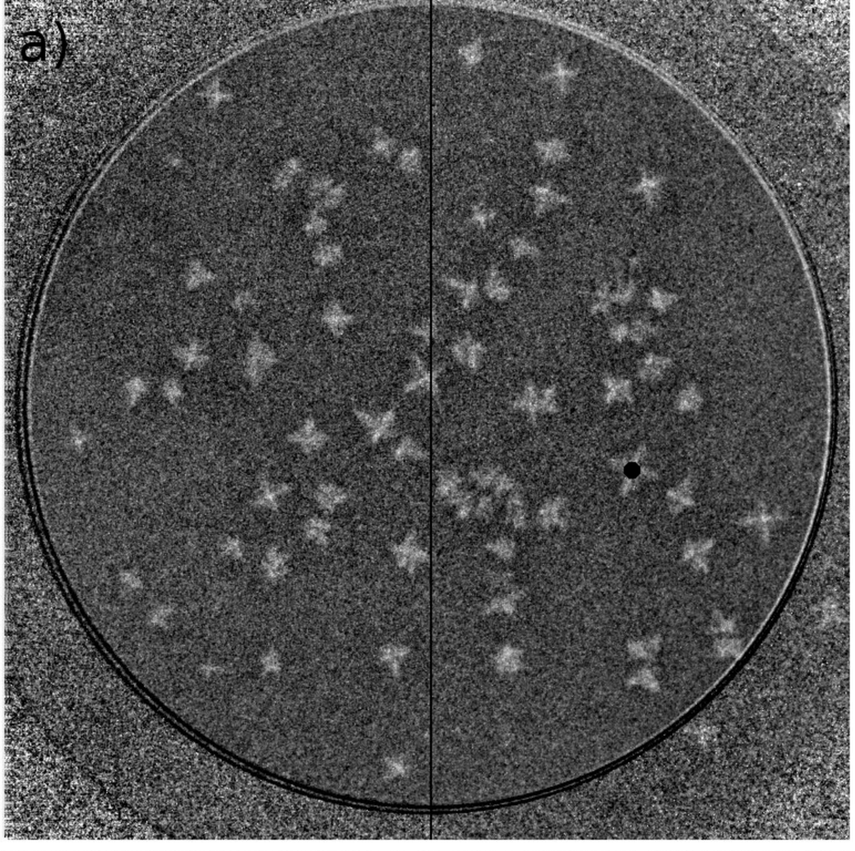
a)

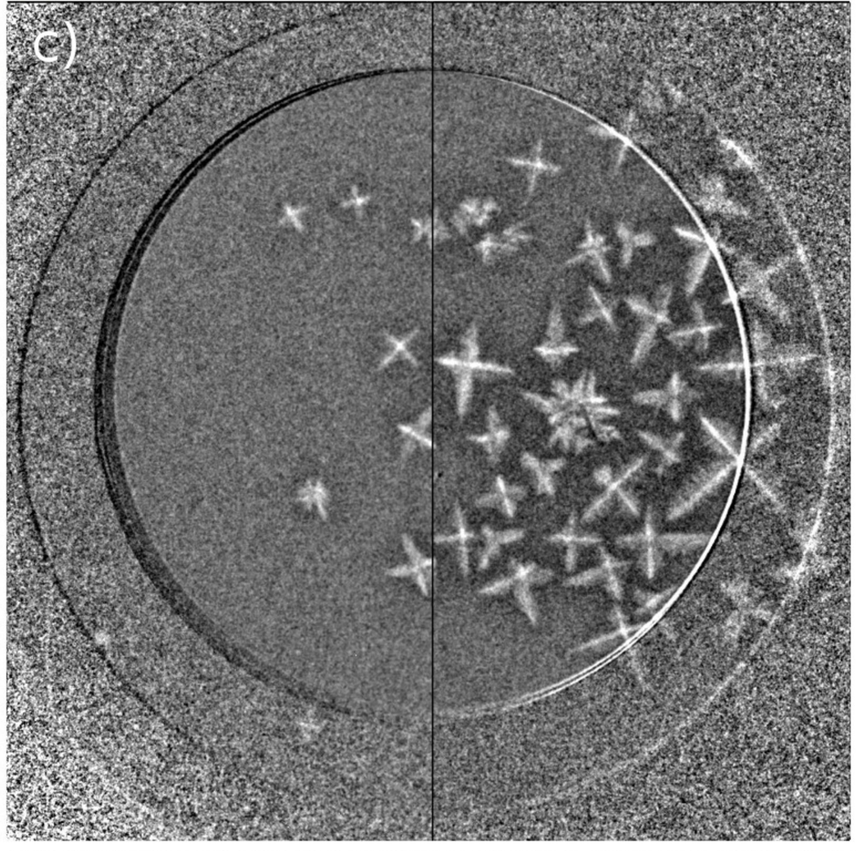
c)

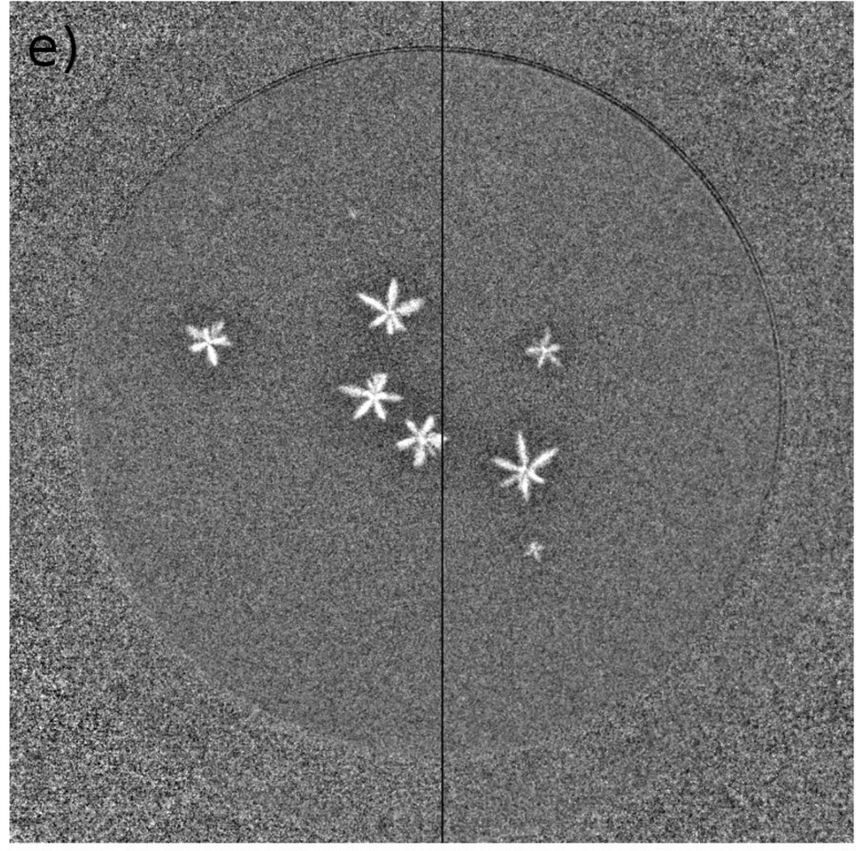
e)

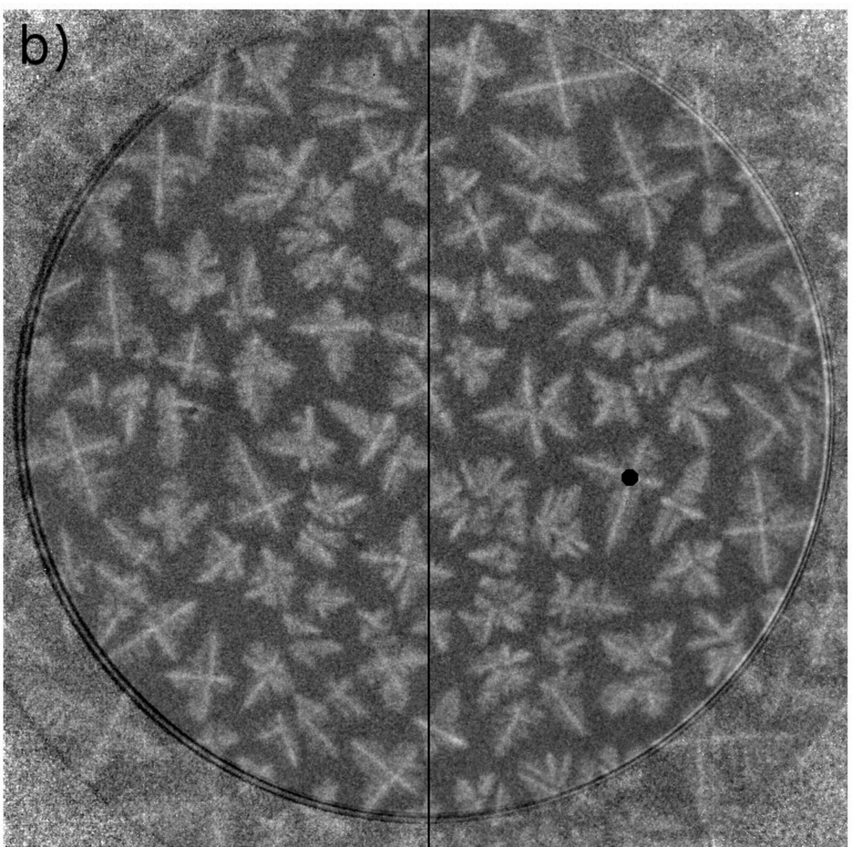
b)

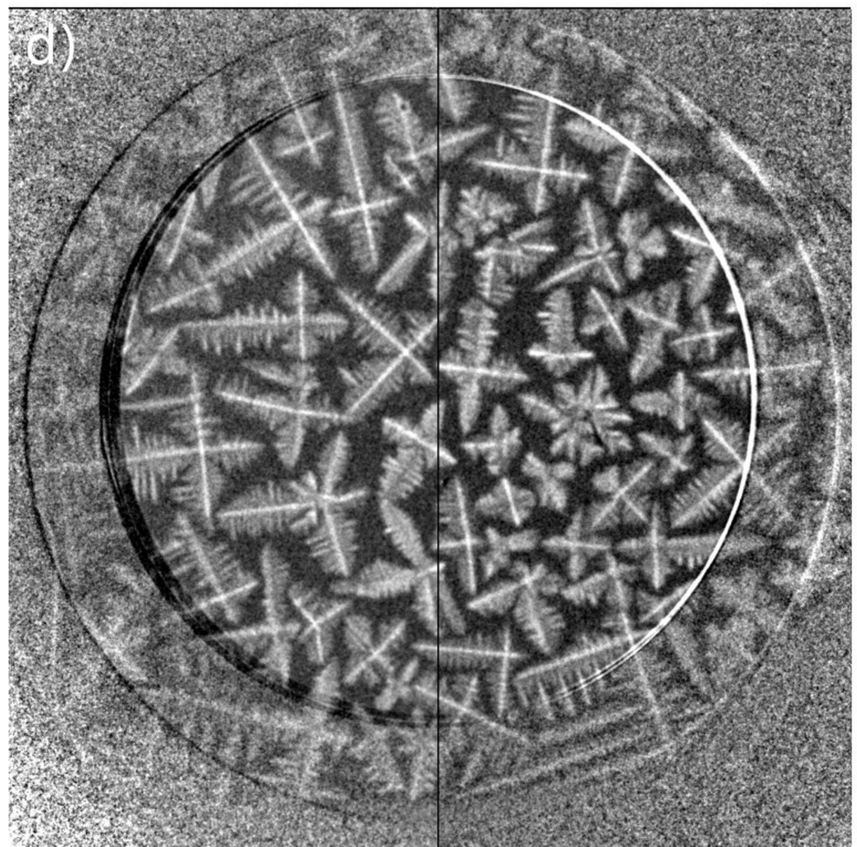
d)

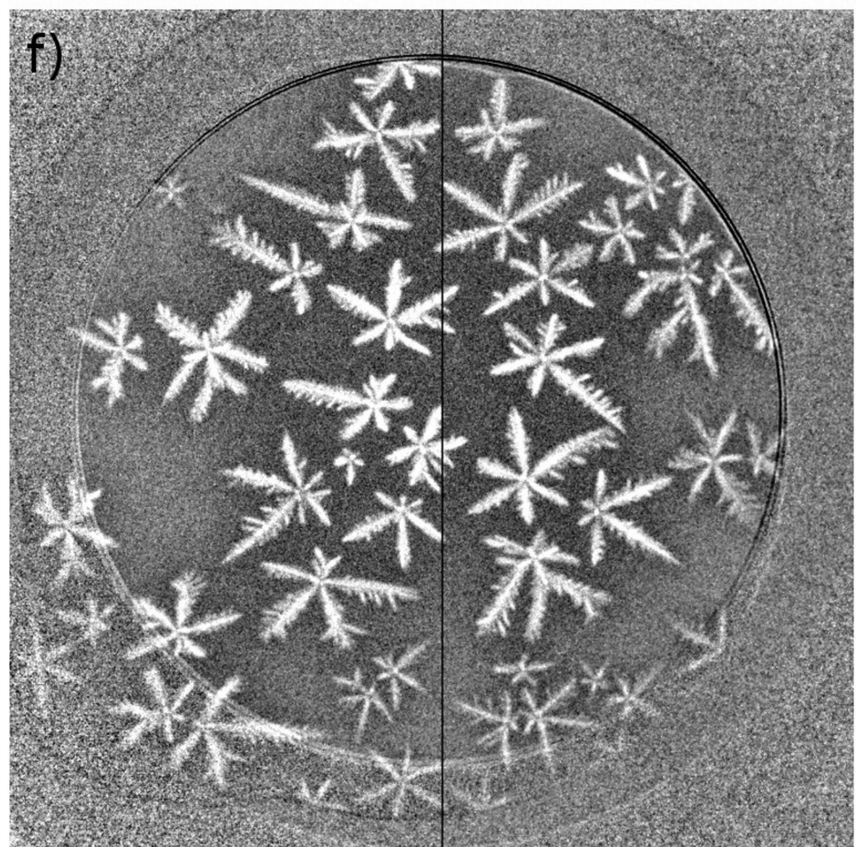
f)

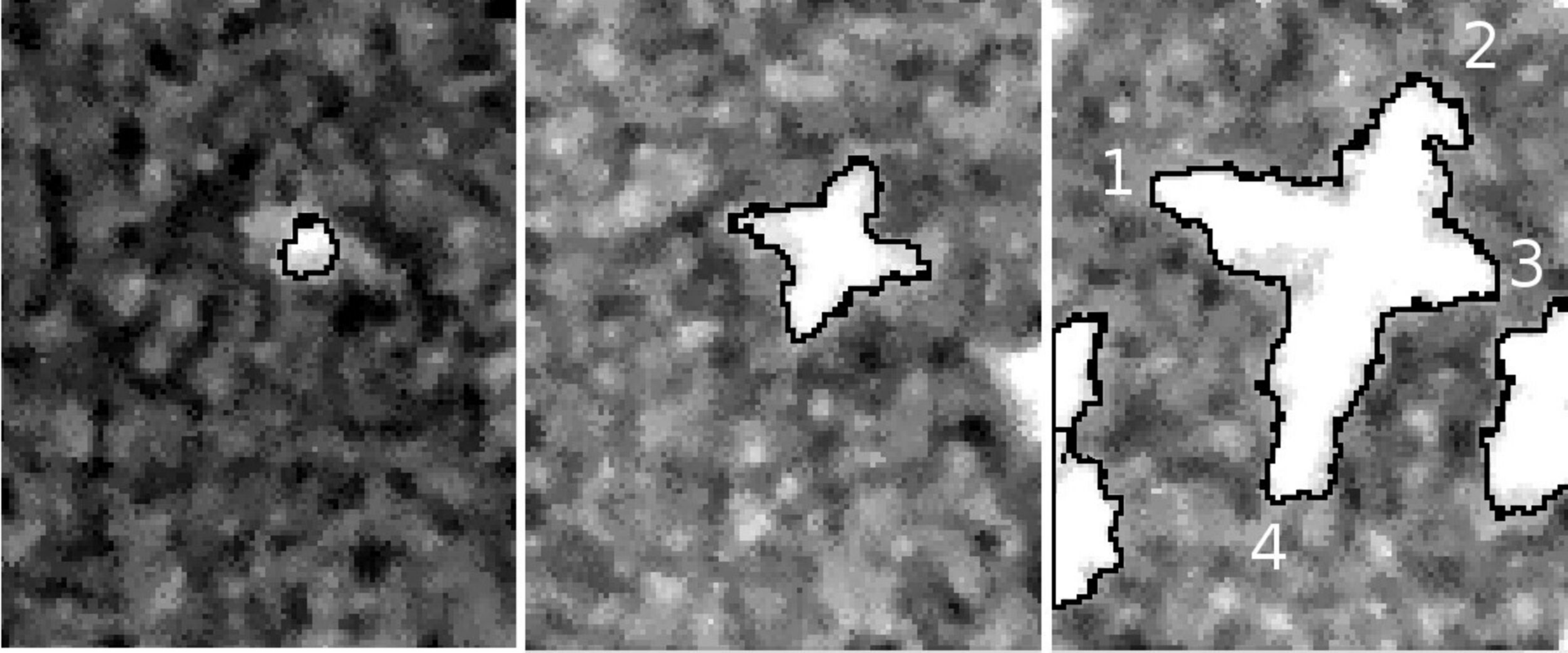
2
1
3
4

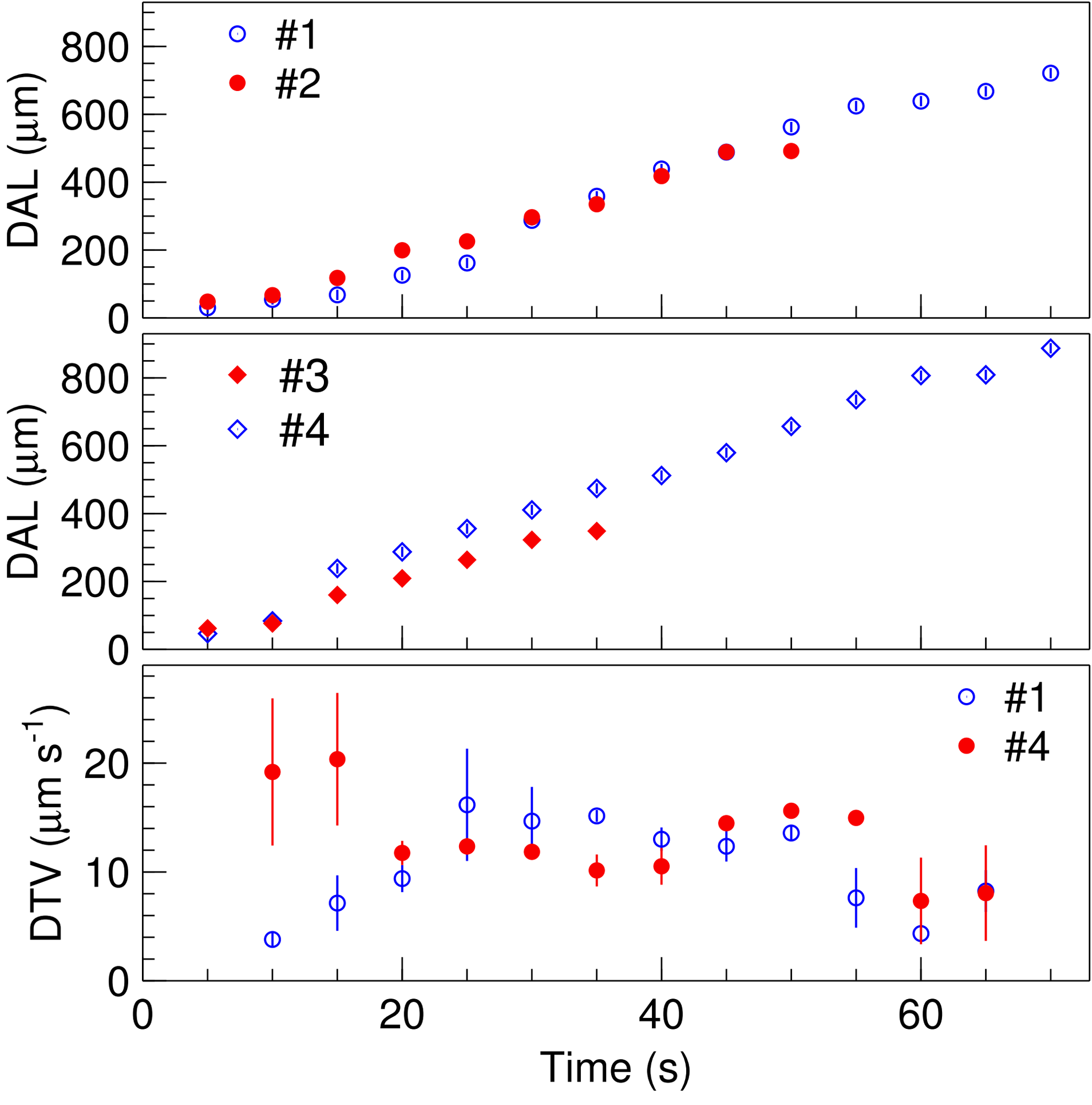
#1
#2
DAL (μm)
0
200
400
600
800
#3
#4
DAL (μm)
0
200
400
600
800
#1
#4
DTV (μm s-1)
0
10
20
0
20
40
60
Time (s)